JOURNAL OF GEOPHYSICAL RESEARCH, VOL. 113, E11005, doi:10.1029/2008JE003104, 2008

Tyrrhena Patera: Geologic history derived from *Mars Express* High Resolution Stereo Camera

David A. Williams,[1] Ronald Greeley,[1] Stephanie C. Werner,[2,3] Greg Michael,[2] David A. Crown,[4] Gerhard Neukum,[2] and Jouko Raitala[5]

Received 5 February 2008; revised 27 June 2008; accepted 8 September 2008; published 7 November 2008.

[1] We used *Mars Express* High Resolution Stereo Camera images of the Tyrrhena Patera volcano to assign cratering model ages to material units defined in the *Viking Orbiter*-based geologic mapping. Cratering model ages are generally consistent with their stratigraphy. We can identify three key intervals of major activity at Tyrrhena Patera: (1) formation of the volcanic edifice in the Noachian Period, ~3.7–4.0 Ga, shortly following the Hellas impact (~4 Ga) and coincident with the formation of Hadriaca Patera (~3.9 Ga); (2) modification of the edifice and formation of the caldera rille and channels in the Hesperian Period, possibly extending into the Amazonian Period; and (3) a final stage of modification in the Late Amazonian Epoch, ~0.8–1.4 Ga. Early- to mid-Hesperian activity on Tyrrhena Patera is consistent with similar activity on Hadriaca Patera at ~3.3–3.7 Ga. The most recent dateable event on Tyrrhena Patera is modification on the upper shield, caldera rille, and channel floors at ~800 Ma. This coincidence of resurfacing in three units suggests a widespread process(es), which we speculate involved preferential (aeolian?) erosion of small craters on these flatter surfaces relative to the other units on the volcano. Alternatively, some combination of pyroclastic flow emplacement on the upper shield and fluvial activity in the caldera rille and channels, followed by differential aeolian erosion and deposition, could have produced the present surface. Regardless, major geologic resurfacing ended at Tyrrhena Patera nearly a billion years ago.

Citation: Williams, D. A., R. Greeley, S. C. Werner, G. Michael, D. A. Crown, G. Neukum, and J. Raitala (2008), Tyrrhena Patera: Geologic history derived from *Mars Express* High Resolution Stereo Camera, *J. Geophys. Res.*, *113*, E11005, doi:10.1029/2008JE003104.

1. Introduction

[2] One of the objectives of the High Resolution Stereo Camera (HRSC) experiment on the European Space Agency (ESA) *Mars Express* orbiter [*Neukum et al.*, 2004a; *Jaumann et al.*, 2007] is to identify a chronology of major events that formed Martian surface features covering large areas using impact crater statistics [e.g., *Hartmann*, 1966; *Neukum and Wise*, 1976]. This includes the timing of eruptions and the formation of major volcanoes, lava flow fields, and pyroclastic deposits. Initial results were presented for the Tharsis and Elysium volcanoes [*Neukum et al.*, 2004b]. Our focus here is on the ''highland paterae'', a group of low-relief volcanoes with unique morphologies located on the margins of the Hellas basin [*Peterson*, 1978; *Schultz*, 1984]. Previous work identified the chronology of major events at Hadriaca Patera [*Williams et al.*, 2007]. The purpose of this paper is to present a geologic history of major events that formed and modified Tyrrhena Patera using crater statistics, based on the previous geologic mapping of *Gregg et al.* [1998].

2. Background

[3] Martian highland paterae are thought to be among the oldest central-vent volcanoes on Mars [*Scott and Carr*, 1978]. These volcanoes have shallow, central caldera complexes on low-relief, deeply dissected slopes exhibiting radial ridges and channels [*Plescia and Saunders*, 1979; *Greeley and Spudis*, 1981]. The main edifices of Hadriaca and Tyrrhena Paterae contain few primary lava flow features; along with the nature of their eroded flanks, this suggests that they are composed of friable deposits, most likely formed by gravity-driven pyroclastic flows [*Greeley and Spudis*, 1981; *Crown and Greeley*, 1993]. Results from recent modeling of pyroclastic flow emplacement [*Greeley and Crown*, 1990; *Crown and Greeley*, 1993; *Gregg and Crown*, 2004; *Gregg and Farley*, 2006] and geologic mapping [*Greeley and Crown*, 1990; *Crown and Greeley*, 2007] support this hypothesis.

[1] School of Earth and Space Exploration, Arizona State University, Tempe, Arizona, USA.
[2] Institute of Geological Sciences, Freie Universität, Berlin, Germany.
[3] Now at Geological Survey of Norway, Trondheim, Norway.
[4] Planetary Science Institute, Tucson, Arizona, USA.
[5] Planetology Group, University of Oulu, Oulu, Finland.

0148-0227/08/2008JE003104$09.00

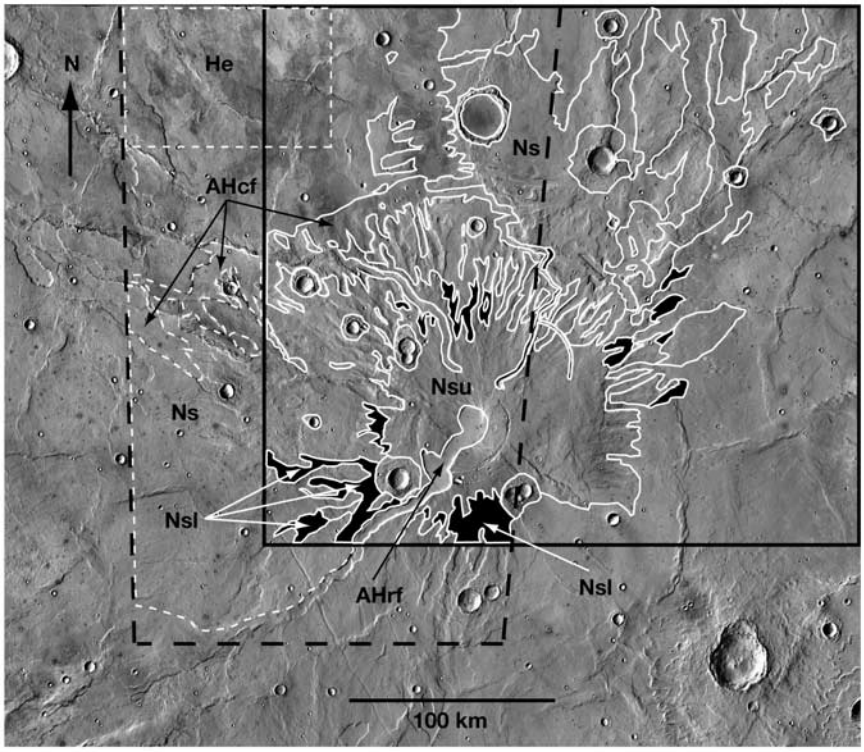

Figure 1. THEMIS daytime-infrared mosaic of the Tyrrhena Patera region (spatial resolution 100 m/pixel). The solid black boundary marks the approximate region of the geologic map of *Gregg et al.* [1998] (their map has additional coverage to the north and east), inside which is a simplified sketch map of the unit contact boundaries (solid white lines) from their map for the six units of interest in this study (labeled). The areas with solid white boundaries and solid black fill are regions of unit Nsl. The dashed black boundary marks the HRSC imaging coverage on which the new crater counts were performed, and the dashed white lines mark extension of the map units of *Gregg et al.* [1998] for crater counting (cf., Figure 2).

[4] Using *Viking Orbiter* images, *Gregg et al.* [1998] produced a geologic map of the summit region of Tyrrhena Patera volcano. They defined and characterized eleven material units related to various volcanic, gradational, and impact crater materials. Here, we use HRSC images to examine six of these units for cratering age assessment. Figure 1 shows a Thermal Emission Imaging System (THEMIS: *Christensen et al.* [2004]) mosaic of the Tyrrhena Patera region (spatial resolution 100 m/pixel), including a simplified sketch map of the unit contact boundaries from the map of *Gregg et al.* [1998] for the six units of interest, relative to the HRSC imaging coverage on which the crater counts were performed.

3. HRSC Imaging

[5] The HRSC imaged Tyrrhena Patera during orbits 440 (25 May 2004), 1909 (11 July 2005), 1920 (14 July 2005), 4195 (12 April 2007), 4206 (15 April 2007), and 4217 (18 April 2007). Orbit 440 covered the caldera and west flank of the volcano, with nadir imaging at 36 m/pixel (Figure 2). During this orbit, corresponding stereo images were obtained at 72 m/pixel, and 4 color images at 144 m/pixel. Orbit 1909 covered east flank of the volcano, with nadir imaging at 30 m/pixel, with corresponding stereo imaging at 60 m/pixel, and with 4 color images at 90 m/pixel. Orbit 1920 was a full-resolution stereo observation that covered the central caldera and flanks of the volcano at 28 m/pixel. Super Resolution Camera (SRC) mosaics were obtained on orbits 1909 and 1920 with nominal resolution of 5 m/pixel, but the actual resolution is reduced by blurring because of an astigmatism in the primary lens caused by thermal imbalance [*Oberst et al.*, 2008]. Later HRSC coverage on orbits 4195, 4206, and 4217 include a series of full-resolution stereo observations (spatial resolutions of 12–13, 13–14, and 13–15 m/pixel, respectively) that are repeat coverage of earlier imaging.

4. Crater Counting Methodology

[6] A film transparency with the six units identified (Figure 2) was produced from the HRSC data and examined by one of us (SCW) under a Zeiss PSK-2 stereo comparator. Crater diameters were measured and partitioned into size bins based on standard practices [e.g., *Crater Analysis Techniques Working Group*, 1979]. The binned data were processed to obtain cumulative crater size-frequency (SF) distributions with corresponding statistical errors [e.g., *Hartmann*, 1966; *Neukum and Wise*, 1976; *Neukum and Hiller*, 1981; *Neukum*, 1983]. Cratering model ages were obtained by fitting the crater production function [*Hartmann and Neukum*, 2001] to the distributions using a non-linear least-squares fitting procedure (following *Marquardt* [1963] and *Levenberg* [1944]), and referring the cumulative crater

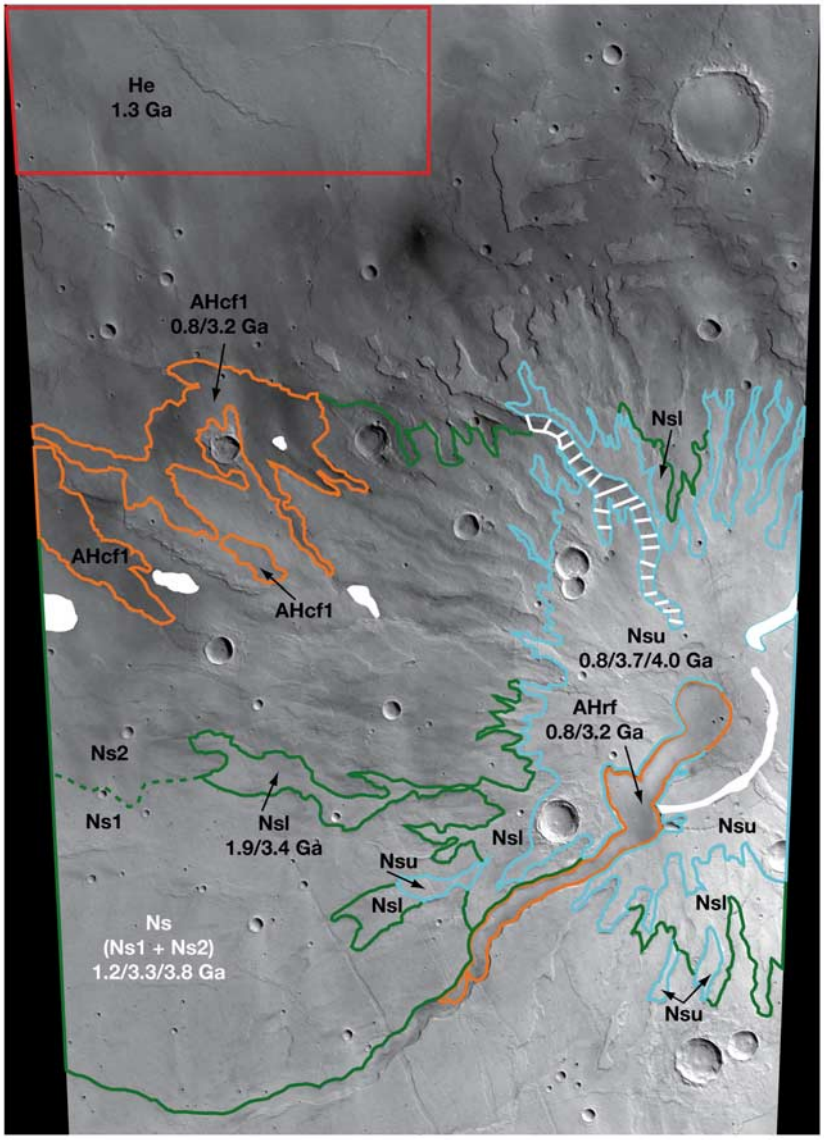

Figure 2. Crater count areas and cratering model ages obtained for Tyrrhena Patera using the techniques described in the study of *Hartmann and Neukum* [2001]. Base map is HRSC image h04400_0000.nd3 with a resolution of 36 m/pixel. Colors delineate different count areas. Filled white and dashed white regions are uncounted. See Table 1 and Figures 3 and 4 for additional information on crater statistics.

density at the reference diameter of 1 km to an established cratering chronology model for Mars [*Neukum*, 1983; *Hartmann and Neukum*, 2001; *Ivanov*, 2001].

[7] The model by *Neukum* [1983] was extrapolated from the lunar model, in which crater frequencies are correlated with radiometric ages from *Apollo* samples. The lunar model was adjusted for the different orbital parameters, crater scaling, and impact flux for Mars relative to the Moon. The transfer of the lunar cratering chronology model to Mars results in a typical uncertainty in cratering model ages by a factor of 2 for ages <3.5 Ga (in the constant flux range), whereas the uncertainty is about ±100 Ma for ages >3.5 Ga [*Hartmann and Neukum*, 2001]. However, testing and application of these techniques shows that the applied Martian cratering chronology model results in ages for basin formation and volcanic surfaces that are in good agreement with Martian meteorite crystallization ages with respect to "peak" activity periods [*Neukum et al.*, 2007]. This suggests that the model is correct within an uncertainty of less than 20% [*Werner*, 2005]. Furthermore, all crater sizes were measured by a single technician in a single image/region, thus ensuring that any difference in the measured crater frequencies indicates an absolute age difference, with a much smaller error range than implied by the chronology model. Therefore the errors are reduced to the statistical error inherent in our measurements, leading to an error roughly of ±100 Ma. Specific 1-sigma standard deviation (SD) error bars for each cratering model age are included in Table 1 and Figure 3.

[8] In recent years there has been an ongoing discussion [*Hartmann*, 2005] about the use of small craters in cratering statistics; specifically, whether it is appropriate to count craters $\leq$300 m diameter because they might be distant secondary craters rather than primary craters [*McEwen et*

Table 1. Crater Count Statistics for Ages of Tyrrhena Patera Units Using HRSC Orbit 440 Nadir Image and Technique Described by *Hartmann and Neukum* [2001] and *Michael and Neukum* [2007][a]

Unit	Name	Area (km^2)	Number of Craters	Crater Size Range for Age Estimate (km)	Cumulative Crater Density $N(1)$	$N(1)$ Error (±)	Cumulative Crater Density $N(10)$	$N(10)$ Error (±)	Cratering Model Age t (Ga), + Error, − Error
AHrf	Rille floor material	346.2	45						
	Formation age		6	0.5–0.9	1.63e − 3	±6.6e − 4	2.33e − 5	±9.4e − 6	3.2 (+0.3, −1.2)
	Resurfacing age		19	0.25–0.4	3.88e − 4	±9.2e − 5	5.54e − 06	±1.3e − 6	0.8 (±0.2)
AHcf	Channel floor material	935.4	55						
	Formation age		2	0.9–1.2	1.63e − 3	±1.1e − 3	2.33e − 5	±1.6e − 5	3.2 (+0.4, −2.1)
	Resurfacing age		22	0.3–0.5	4.0e − 4	±8.4e − 5	5.71e − 6	±1.2e − 6	0.8 (±0.2)
He	Etched plains material	2,160	200	0.3–1.1	6.5e − 4	±6.6e − 5	9.29e − 6	±9.4e − 7	1.3 (±0.2)
Nsu	Upper shield material	2,746	335						
	Formation age		4	4–7	3.23e − 2	±1.6e − 2	4.61e − 4	±2.3e − 4	4.0 (+0.06, −0.1)
	Resurfacing age		8	1–1.5	4.83e − 3	±1.5e − 3	6.90e − 5	±2.1e − 5	3.7 (+0.06, −0.09)
	Resurfacing age		243	0.2–0.5	3.74e − 4	±2.5e − 5	5.35e − 6	±3.6e − 7	0.8 (±0.05)
Nsl	Lower shield material	1,154	166						
	Resurfacing age		5	0.8–1.5	2.32e − 3	±1.0e − 3	3.31e − 5	±1.5e − 5	3.4 (+0.1, −0.8)
	Resurfacing age		61	0.3–0.5	9.48e − 4	±1.1e − 4	1.35e − 5	±1.6e − 6	1.9 (±0.2)
Ns	Basal shield material	8,099	871						
	Formation age		5	3–5	0.0106	0.0047	0.000151	6.7e − 005	3.8 (+0.06, −0.1)
	Resurfacing age		25	0.8–1.2	0.00181	0.00054	2.59e − 005	7.7e − 006	3.3 (+0.2, −0.7)
	Resurfacing age		528	0.25–0.5	0.000575	3.9e − 005	8.22e − 006	5.6e − 007	1.2 (±0.08)

Notes: $N(1)$ = cumulative number of craters with diameters ≥1 km per km^2. $N(10)$ = cumulative number of craters with diameters ≥10 km per km^2. N error bars = $\pm N(x)/\mathrm{sqrt}(n)$. sqrt = Square root. n = Number of craters counted [*Crater Analysis Techniques Working Group*, 1979]. Cratering model age for formation events calculated from Martian chronology model of *Neukum* [1983], , and *Ivanov* [2001]: $N(1) = 2.68 \times 10^{-14}[e^{6.93t} - 1] + 4.13 \times 10^{-4} t$. For method of resurfacing age determination, see the study of *Michael and Neukum* [2007].

[a]Refer to Figures 1 and 2 for count areas, Figure 3 for cumulative size-frequency plots. Crater densities normalized per square kilometer.

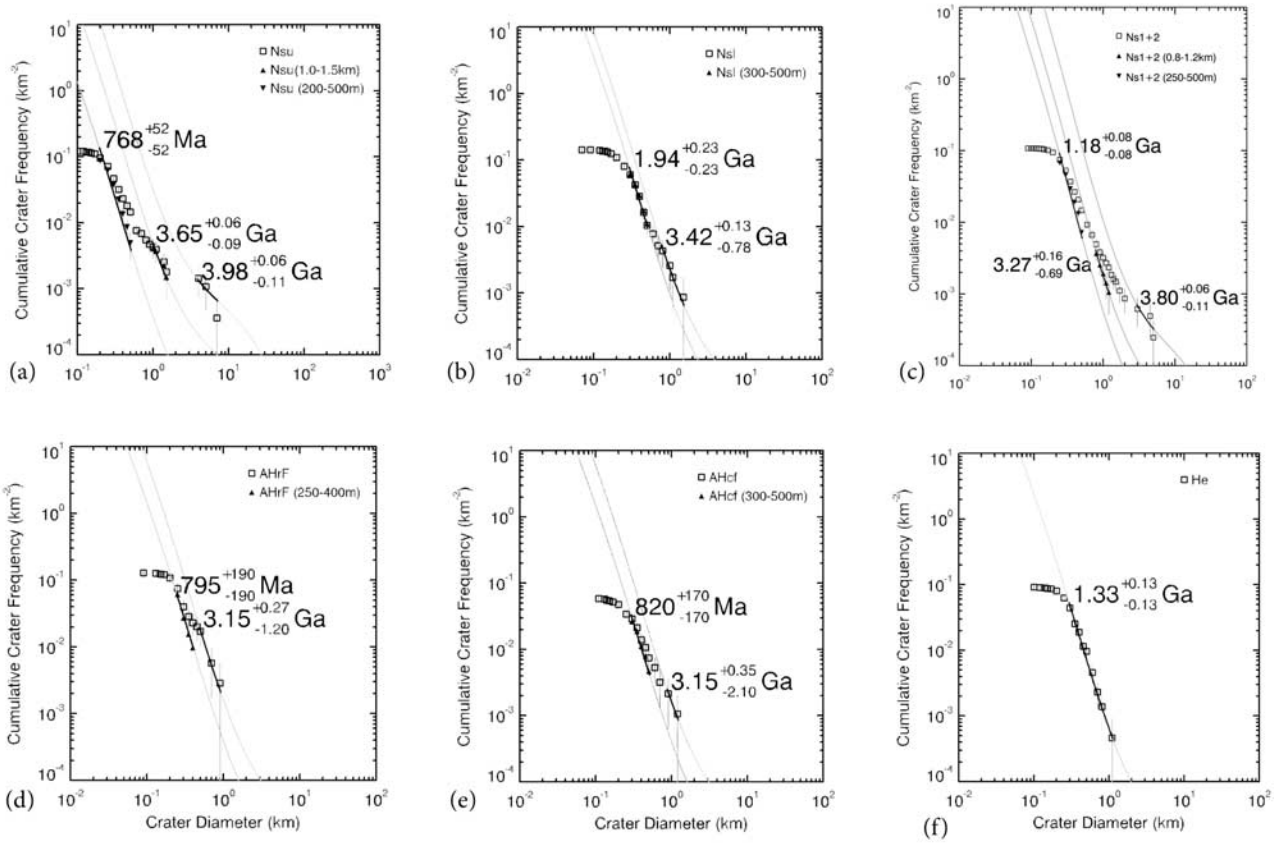

Figure 3. Cumulative crater size-frequency plots showing crater distributions and cratering model ages obtained for Tyrrhena Patera units using the techniques described in the studies of *Hartmann and Neukum* [2001] and *Michael and Neukum* [2007]. (a) Unit Nsu. (b) Unit Nsl. (c) Unit Ns. (d) Unit AHrf. (e) Unit AHcf. (f) Unit He. Dates and error bars given to two decimal places to be consistent with *Neukum et al.* [2004b]; however, for the nature of our discussion in the text, dates and errors are rounded to one decimal place. See Tables 1 and 2 and Figure 4 for additional information on crater statistics.

al., 2005]. In our previous studies, we have not found any deviation in the size-frequency curve steepness between measured and predicted crater size-frequency distributions, except for resurfacing 'kinks', even down to crater sizes of about 100 m diameter [e.g., *Hartmann et al.*, 2008]. Recently *Malin et al.* [2006] estimated the current Martian cratering rate, based on changes observed in MOC images over a seven year period, and they found that the models that scale lunar cratering rates to Mars are consistent with the observed Martian cratering rate [*Hartmann*, 2007; *Hartmann et al.*, 2008].

[9] The crater SF data for complex surfaces typically require multiple curve fits, because of one or more slope breaks in the size-frequency distribution curve [e.g., *Neukum and Hiller*, 1981; *Werner*, 2005]. These kinks are interpreted to represent changes in the crater distribution due to the emplacement of new material (e.g., covering by new volcanic flows or aeolian deposits) or the degradation of existing material (e.g., by fluvial or aeolian erosion). Thus a calculated model age may mark the end of a period of significant resurfacing, caused by erosion or deposition.

[10] New piece-wise fitting methods yield a refined cratering model age to identify the end of resurfacing. The procedure involves fitting the known crater production function to an interval of the crater size range (D_{min}, D_{max}) that is interpreted to represent the accumulation of craters since the resurfacing event. Typically, this is seen as a portion of the cumulative frequency curve that is of constant gradient, but slightly shallower than the production function. The change of gradient is caused by the excess contribution of the larger and older craters whose presence was either less affected, or entirely unaffected, by the resurfacing event. If left uncorrected, that contribution produces an overestimate of the age of the resurfacing event. It is possible to exclude the craters of diameter above D_{max} from the counts [*Neukum and Hiller*, 1981], but this leads to the opposite effect: the gradient becomes steeper than the production function because of the absence of the contribution from larger craters formed after the resurfacing event, and thus the derived age becomes an underestimate.

[11] The known production function describes the number of craters $N(D)$ larger than diameter D relative to $N(D^*)$ for any other diameter, D^*. This means that we have a known slope for the curve within the interval, but the absolute values of $N(D)$ are not known. By varying the absolute value of $N(D_{max})$ with an iterative procedure, it is possible to find the value where the slope of the observed interval ($N(D_{min})$, $N(D_{max})$) best fits the slope of the

Table 2. Adjustment Parameters for Resurfacing Age Determination for Tyrrhena Patera Units[a]

Unit	Slope Fit Range Min (km)	Slope Fit Range Max (km)	$N(D_{max})$ Raw (/km^2)	$N(D_{max})$ Adjusted (/km^2)
Nsu	1	1.5	0.00182	0.00151
Nsu	0.2	0.5	0.0146	0.00499
Nsl	0.3	0.5	0.0104	0.0111
Ns	0.8	1.2	0.00235	0.00104
Ns	0.25	0.5	0.0147	0.00722
AHrf	0.25	0.4	0.023	0.00974
AHcf	0.3	0.5	0.00749	0.00471

[a]Refer to Table 1 and Figure 3. After the study of *Michael and Neukum* [2007].

production function, and thus obtain the absolute value of $N(D_{max})$ (Table 2). This value describes the population of craters larger than D_{max} that would be consistent with the observed population within the interval (D_{min}, D_{max}) [*Michael and Neukum*, 2007; *Michael and Neukum*, in preparation]. In cases where additional resurfacing processes took place, the correction has to be repeated at the next cut-off diameter [*Werner*, 2005]. This procedure was used to determine all of the resurfacing ages given in Table 1 and Figure 3, where the adjusted portion of the crater distribution is indicated by solid triangle symbols.

5. Results

[12] We assessed the ages for the upper summit, lower summit, and basal shield materials, caldera rille floor materials, channel-floor materials, and adjacent Hesperian etched plains materials. Figure 2 shows the crater count regions and resulting cratering model ages (compare with Figure 1), Figure 3 shows the cumulative crater SF plots for each unit, and Tables 1 and 2 contain the numerical results for total craters counted, $N(1)$ retention ages, cratering model ages, and corresponding error bars. Figure 4 shows the cratering model ages with 1-sigma error bars in a graphical format relative to the Martian geologic timescale. We now report the results of the cratering statistics for each of the six units.

5.1. Upper Summit Shield Materials (Unit Nsu)

[13] *Description:* This unit is smooth (at the 50 m/pixel scale) and continuous, forming isolated mesas surrounded by lower summit and basal shield materials [*Gregg et al.*, 1998]. It contains steep, amphitheater-shaped scarps facing away from the summit, forming the headwalls of wide, flat-floored channels oriented radial to the summit. It also contains crater chains, arcuate graben, radial (to the summit) mare-type ridges and concentric narrow arcuate ridges, but lacks fully developed, flat-floored, steep-walled channels [*Gregg et al.*, 1998]. *Interpretation:* This unit is likely pyroclastic flow deposits erupted from Tyrrhena Patera, in which the pit crater chains and arcuate graben mark the collapse zone around the summit produced by magma withdrawal or eruption [*Gregg et al.*, 1998]. *Greeley and Crown* [1990] also suggested that lava flows, now buried by aeolian materials, may cap the summit region. *Age*

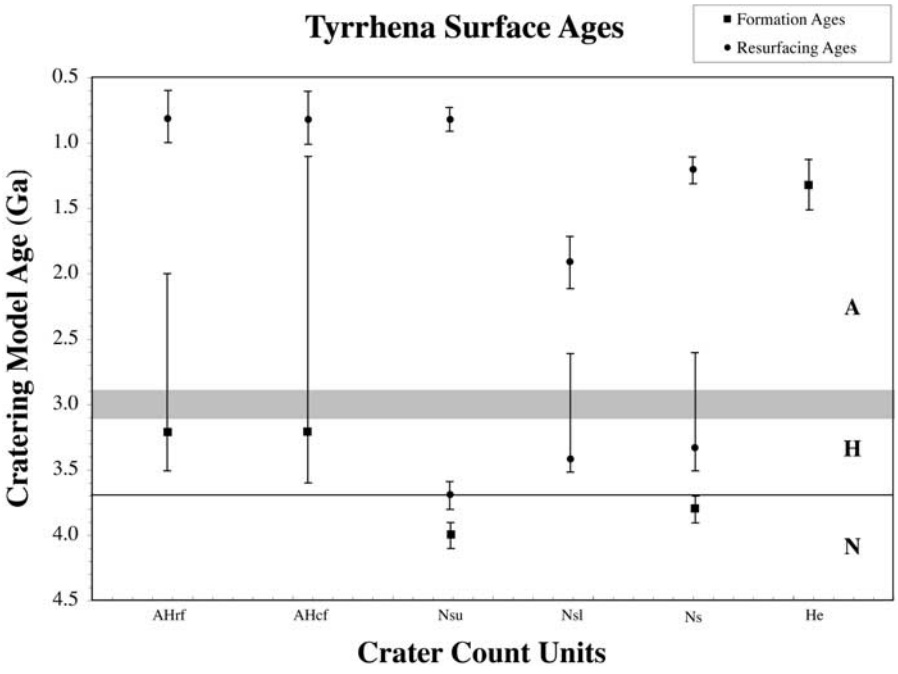

Figure 4. Graph of Tyrrhena Patera age data for various crater count units. Cratering model ages (with 1-sigma standard deviation error bars) plotted relative to the Martian geologic timescale of *Hartmann and Neukum* [2001]. The gray bar represents the uncertainty in position of the Hesperian-Amazonian boundary as determined by the different Hartmann and Neukum methodologies. From this plot, it is clear that there are three grouping of age dates: (1) formation of Tyrrhena Patera's summit and flanks in the Noachian Period; (2) formation of the caldera rille, channel floors, and modification of some flank units in the Hesperian Period; and (3) modification/resurfacing of most regions of Tyrrhena Patera by various processes in the Late Amazonian Epoch.

Figure 5. HiRISE image PSP_001674_1610 of the etched plains material (unit He) of *Gregg et al.* [1998]. Small linear duneforms are scattered across a cratered and pitted surface. The provenance of this surface has been difficult to determine given subsequent modification, although recent work suggests that it is composed of thin lava flows originating NE of the Tyrrhena Patera edifice in Hesperia Planum (T. K. P. Gregg, personal communication, 2008). Scale bars is 500 m. Image courtesy of HiRISE Team.

Assessment: Our crater count results show kinks in the size-frequency curve indicative of multiple resurfacing events, in which "resurfacing" can be caused by deposition of new material and/or erosion of the existing material (Figure 3a). For unit Nsu we find a formation age of 4.0 Ga, with two distinct resurfacing events at 3.7 Ga and 0.8 Ga.

5.2. Lower Summit Shield Materials (Unit Nsl)

[14] *Description:* This unit is a discontinuous, smooth to locally hummocky surface, with isolated steep-sided mesas and spurs surrounded by basal shield materials [*Gregg et al.*, 1998]. It also contains relatively narrow (<500 m wide), V-shaped, slightly sinuous channels, and it is defined in part by steep to shallow scarps facing away from the summit [*Gregg et al.*, 1998]. *Interpretation:* This unit is pyroclastic deposits erupted from Tyrrhena Patera that are more modified by erosional activity than unit Nsu, perhaps by groundwater sapping (based on scarp distribution and morphology) [*Gregg et al.*, 1998]. *Age Assessment:* We obtained a cratering model age of 3.4 Ga, (which, as we discuss later, cannot be a formation age, based on the ages of stratigraphically higher and lower units, but rather a resurfacing age), with another resurfacing age of 1.9 Ga for this unit (Figure 3b).

5.3. Basal Shield Materials (Unit Ns)

[15] *Description:* This unit has a smooth surface, discontinuous around the overlying units up to ~200 km from the summit, that is heavily dissected by ~5 km wide, flat-floored channels [*Gregg et al.*, 1998]. It occurs as isolated, steep-sided mesas surrounded by channel floor materials or plains materials, or as the floors of some broad channels [*Gregg et al.*, 1998]. It contains steep scarps that often contain two or more slope breaks, which they used to help define unit boundaries. *Interpretation:* This unit is pyroclastic deposits from Tyrrhena Patera, heavily modified by groundwater sapping, with local morphologic variations resulting from differential erosion or separate eruptive events [*Gregg et al.*, 1998]. *Age Assessment:* We found a cratering model formation age of 3.8 Ga for unit Ns (= Ns_1 + Ns_2: see below), with resurfacing ages of 3.3 Ga and 1.2 Ga (Figure 3c). However, in *Viking Orbiter*-based regional mapping, *Greeley and Crown* [1990] divided this region into basal shield materials and a smooth plains unit interpreted to be either a facies of the surrounding ridged plains or a volcanic unit at the base of Tyrrhena Patera. Our analysis of the HRSC image (Figure 2) also suggests that the southern part of unit Ns (labeled Ns_1 in Figure 2) has a less channeled morphology than the northern part (labeled Ns_2, and sepa-

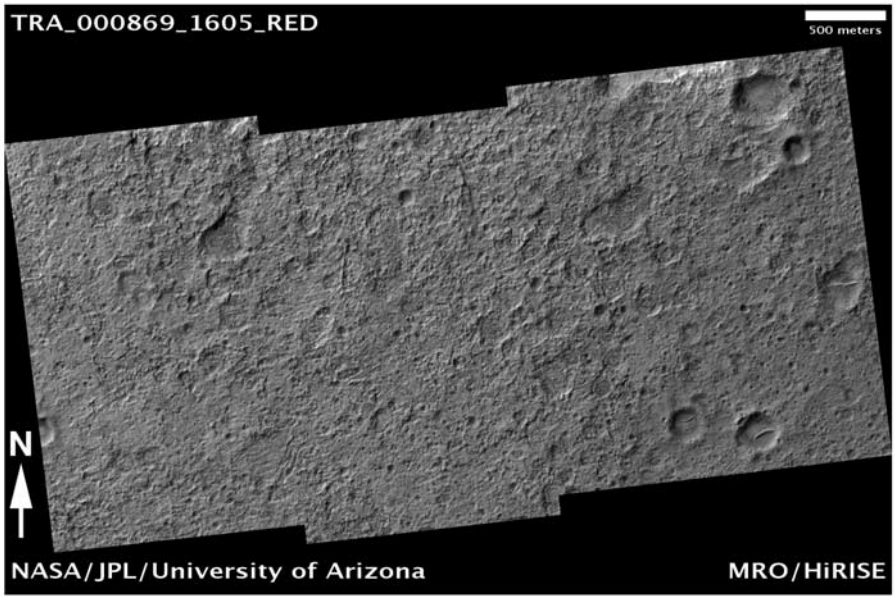

Figure 6. HiRISE image TRA_000869_1605 of the basal shield material (unit Ns) of *Gregg et al.* [1998]. This region is on top of the "E"-shaped mesa north of Tyrrhena Patera. There is a relative dearth of small duneforms superposed on a rough (at the tens of meters scale) and pitted surface. This unit was mapped by *Gregg et al.* [1998] as pyroclastic flow deposits that make up the base of the Tyrrhena Patera volcano. Scale bars is 500 m. Image courtesy of HiRISE Team.

rated by a green dashed line in Figure 2), perhaps indicative of differential erosion on parts of this unit.

5.4. Caldera Rille Floor (Unit AHrf)

[16] *Description:* The rille-like caldera floor of Tyrrhena Patera is the smoothest, least cratered part of the volcano in *Viking*, THEMIS, and HRSC images, and crosscuts the other units of the volcano. *Interpretation:* This unit is interpreted as late-stage lava flows that feed a large (~1000 km by ~200 km) lava flow field southwest of the volcano outside the map area [*Greeley and Crown*, 1990; *Crown et al.*, 1991; *Gregg et al.*, 1998]. *Age Assessment:* The entire central caldera rille was counted as a single unit, because there are no apparent variations in crater abundance or morphology to suggest multiple units. Our crater counts (Figure 3d) indicate that the caldera rille has a formation age of 3.2 Ga, with later resurfacing at 0.8 Ga.

5.5. Channel Floor Materials (Unit AHcf)

[17] *Description:* This unit has a mottled surface locally cut by shallow, narrow (<500 m wide), V-shaped channels within wider (~5 km), steep-walled, flat-floored channels that dissect the shield materials [*Gregg et al.*, 1998]. *Interpretation:* This unit is reworked summit and basal shield materials, which were transported and deposited by fluvial and mass wasting processes [*Gregg et al.*, 1998]. *Age Assessment:* The HRSC images show this unit to be a lower albedo region of eroded plains (Figure 2). We obtained a cratering model age of 3.2 Ga, with a resurfacing age of 0.8 Ga (Figure 3e).

5.6. Etched Plains Materials (Unit He)

[18] *Description:* This unit is a broad, flat, mottled plains generally lacking in mare-type ridges, but with shallow, cuspate scarps in between and parallel to the ridges. In some locations smooth deposits appear to mantle the ridges. It embays the basal shield material west of the summit of Tyrrhena Patera [*Gregg et al.*, 1998]. *Interpretation:* This unit is either thin lava flows or pyroclastic material, with the mantling deposits coming from reworked shield material [*Gregg et al.*, 1998]. *Age Assessment:* We obtained a cratering model age of 1.3 Ga for this unit (Figure 3f), indicating it formed in the Amazonian rather than the Hesperian Period. This is the only significant discrepancy with the stratigraphy of map units from *Gregg et al.* [1998]. *Greeley and Crown* [1990] included this region in their smooth plains unit, with several potential origins and a likely Hesperian age.

6. Discussion and Interpretations

[19] Our cratering model age dates indicate that significant geologic activity on Tyrrhena Patera continued throughout much of Martian history, well into the Amazonian Period. To a first order, our results are consistent with the mapping of *Gregg et al.* [1998]. Only unit He, the etched plains material NW of the volcano, was mapped as Hesperian but has a Amazonian model age. Other studies have had difficulty in identifying the provenance of this unit (Figure 5); recent examination of THEMIS images suggests that unit He is actually composed of thin lobate lava flows that originated somewhere to the NE of the Tyrrhena Patera edifice, and that these flows embay all other units in the map area (T.K.P. Gregg, personal communication, 2008). This result is consistent with the crater statistics shown here.

[20] Cross-comparison of our results (Figures 2–4 and Table 1) shows that there are essentially three key intervals of major activity at Tyrrhena Patera: (1) formation of the volcanic edifice in the Noachian Period, ~3.7–4.0 Ga; (2) modification of the edifice and formation of the caldera

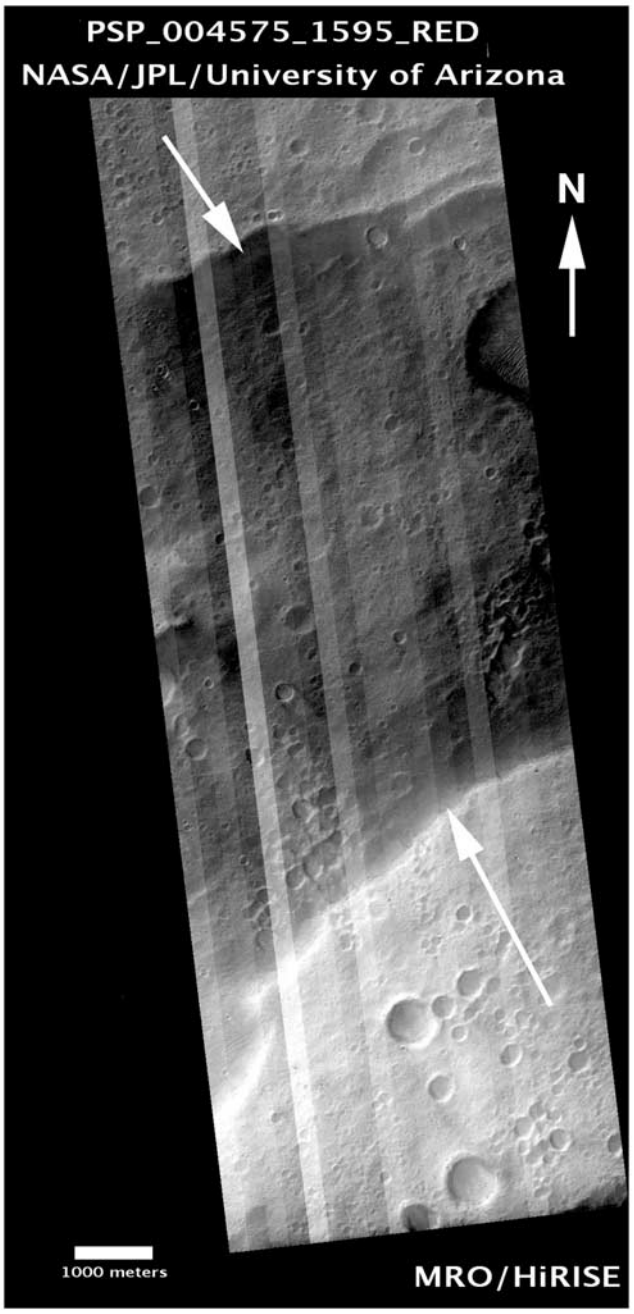

Figure 7. A segment of HiRISE image PSP_004575_1595 covering a section (between white arrows) of the lower shield material (unit Nsl) of *Gregg et al.* [1998]. This region is located on the east side of Tyrrhena Patera and was not counted in our study. Although the quality of this HiRISE image is poor, the surface is cratered and pitted and contains linear duneforms, trending ENE, consistent with the Hellas regional winds, much like the other shield units. This unit was mapped by *Gregg et al.* [1998] as pyroclastic flow deposits that make up the lower parts of the Tyrrhena Patera volcano. Scale bars is 1000 m. Image courtesy of HiRISE Team.

rille and channel floors in the Hesperian Period, ~3.2–3.7 Ga (although error bars suggest activity could have occurred much later in Martian history); and (3) a final stage of modification in the Late Amazonian Epoch, ~0.8–1.4 Ga. Further analysis of our results provides insight into the multiple stages of geologic activity associated with Tyrrhena Patera, including consideration of the type of process or processes that were responsible for modification of the ancient flanks of the volcano. Understanding the geologic record of Tyrrhena Patera in the Amazonian Period has particular importance for constraining the longevity, magnitude, and styles of volcanism in the region as well as its volatile history. The following sections examine specific issues that have arisen from examination of the cratering model ages:

[21] 1. *Stratigraphy vs. Age: Shield units:* Previous studies have suggested Tyrrhena Patera is constructed of multiple pyroclastic flow deposits, which are easier to erode than lava flows [*Greeley and Crown*, 1990; *Crown et al.*, 1992]. The law of superposition says that the oldest units occur on the bottom of a stratigraphic sequence, and get progressively younger with elevation. In the case of the map units by *Gregg et al.* [1998], the basal shield material (unit Ns, Figure 6) is the oldest, followed by the Lower summit shield material (unit Nsl, Figure 7), with the Upper summit shield material (unit Nsu, Figure 8) being the stratigraphically youngest. Yet our cratering model ages of formation for these units are 3.8 Ga (Ns), 3.4 Ga (Nsl), and 4.0 Ga (Nsu). Why does this discrepancy occur? First, further study of the cumulative SF distribution of unit Nsl has identified unusual behavior; at around 500m the curve dips beneath the isochron relative to the curve both above and below this diameter. For this reason, the slope is *steeper* than the isochron in the section we measured previously, and the resurfacing correction therefore produces an older age (because $N(D^*)$ must be increased to match the slope). Recall that unit Nsl is composed of several small patches of the exposure based on the map of Gregg et al. (Figures 1, 2), and that the 3.4 Ga age has a rather large 1-sigma error bar (2.6–3.6 Ga). We suggest that these complexities are a result of crater counting on a selection of separate areas from different locations around Tyrrhena Patera that have actually experienced different erosional histories, and thus our crater statistics are the result of a mixture effect from these units with different histories. Our oldest measurable age of Nsl of 3.4 Ga thus cannot be a true formation age. We suggest that caution should be utilized when considering these unit Nsl age estimates.

[22] Second, when one considers the 1-sigma standard deviation error bar on the stratigraphically-lower unit Ns (3.7–3.9 Ga), we find that this unit has a similar age to the stratigraphically-higher unit Nsu (including its 1-sigma standard deviation error bar: 3.9–4.0 Ga). Thus we suggest both units Ns and Nsu likely formed somewhere ~3.7–4.0 Ga. It is important to remember that these error bars are not hard limits. One cannot say that the true age must lie within these 1-sigma bars but, more precisely, that there is a 68% probability that they do (at least, with regard to the statistical errors that the bars are showing). There is 97.5% probability that the value lies within 2 SD and 99.7% within 3 SD. Thus we suggest that the most useful age constraints that can be reported from these results is that the

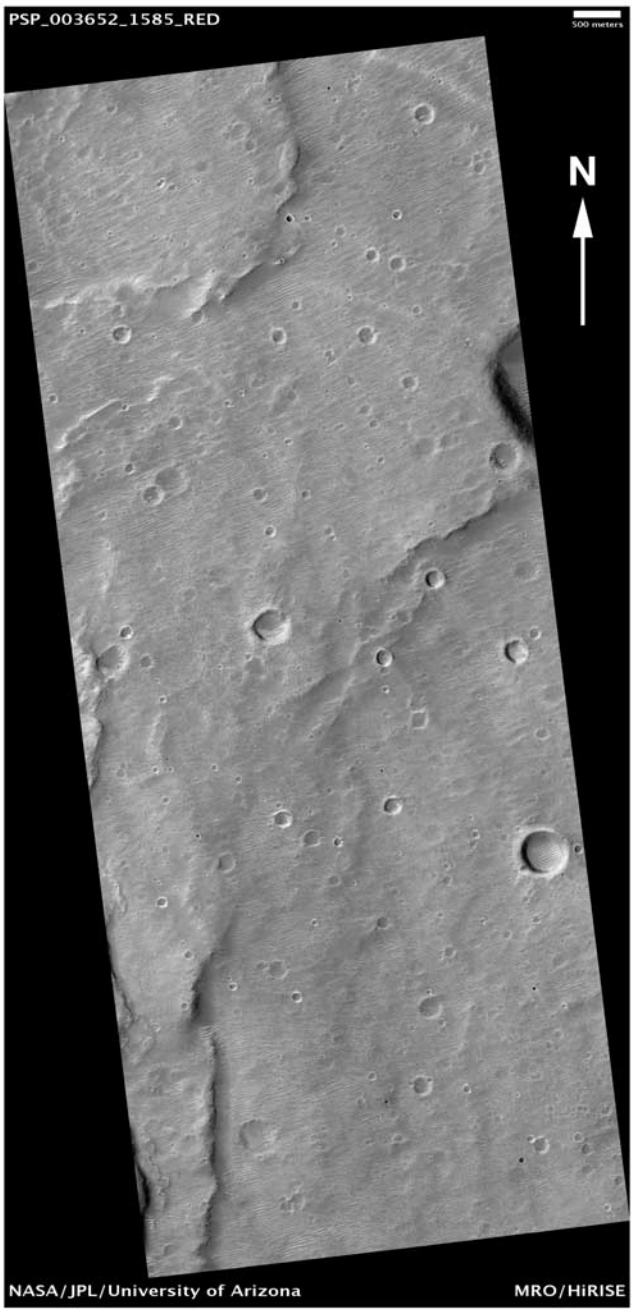

Figure 8. HiRISE image PSP_003652_1585 of the upper shield material (unit Nsu) of *Gregg et al.* [1998]. This region is located just east of the summit caldera and west of the concentric curvilinear fracture. At full HiRISE resolution (30 cm/pixel), the surface is covered by linear duneforms, trending ENE, consistent with the Hellas regional winds. This unit was mapped by *Gregg et al.* [1998] as pyroclastic flow deposits that make up the summit of the Tyrrhena Patera volcano. Scale bars is 500 m. Image courtesy of HiRISE Team.

Tyrrhena Patera edifice (units Ns, Nsl, Nsu) was built by multiple explosive eruptions within a few hundred million year period between ~3.7–4.0 Ga, after the formation of the Hellas impact basin (4.0 Ga [*Werner and Neukum*, 2003; *Werner*, 2005]). These results confirm the extreme age of the Tyrrhena edifice [see also *Crown et al.*, 2005], dating back to the Noachian Period (and consistent within uncertainties with the formation of Hadriaca Patera: 3.9 Ga [*Williams et al.*, 2007]). Additionally, we suggest that the 3.7 Ga age of unit Nsu may represent either resurfacing by additional volcanic eruptions at the Hesperian-Noachian boundary that likely included pyroclastic flows that continued to build the Tyrrhena Patera volcano, and/or represent resurfacing by erosional modification of the Noachian edifice [*Greeley and Crown*, 1990; *Crown and Greeley*, 1993]. If one interprets the Hesperian cratering model ages as evidence of erosion and recognizes the mixture of old and young surfaces on the units defined, then we note that an oldest erosional age of 3.7 Ga is associated with the least dissected of the Tyrrhena Patera map units (i.e., unit Nsu shows an older resurfacing age relative to Nsl and Ns). This point thus could be considered as evidence in support of an erosional interpretation of the resurfacing ages.

[23] 2. *Stratigraphy vs. Age: Caldera and Channel units:* In the map of *Gregg et al.* [1998], the caldera rille material (unit AHrf: Figure 9) and the channel floor material (unit AHcf) cross-cut the other units, such that their formation ages (3.2 Ga +0.4, −2.1 Ga) must be younger than the formation ages of the shield units (3.7–4.0 Ga). This is consistent with our results. However, we find evidence in the crater SF distributions for resurfacing events on unit Nsl at 1.9 Ga and on unit Ns at 1.2 Ga that are not reflected in units AHrf and AHcf. One might expect a resurfacing event to affect all the units around the volcano at the same time, not just some units but not others (except for indurated materials, which might be less affected by an erosional event). Discounting the unit Nsl data because of the complexities discussed earlier, we must ask why does this apparent discrepancy with unit Ns occur?

[24] First, we must be clear regarding our meaning of "resurfacing event". A resurfacing event is a geologic process(es) that removes a portion of the crater population in a given size range. These process(es) all involve some form of material transport, with both erosional and depositional components, either of which can erase cratered surfaces: for example, volcanic eruptions (emplacing lava flows or pyroclastic deposits), catastrophic floods that cut channels or deposit sediment, dust storms that scour a surface or bury craters, etc. Discrete events (like a volcanic eruption or catastrophic flood) should produce a sharp kink in a SF distribution. A rapid event removes the small end of the distribution with a very distinct boundary, i.e., a sharp kink in the SF curve. As the impact population builds up again on the new surface, this sharp kink remains. However, if the resurfacing process is a slower one, e.g., the erosion of high-relief features, the effect is to more quickly remove the population at the small end of the distribution but more slowly in the mid-range, producing a gentle drop-off. If this erosional period ceases, and the population builds up again, the resulting curve shows a gentler transition between the formation and resurfacing periods. Also, it is likely that in early- to mid-Martian history, multiple processes could be operating simultaneously: for example, an erupting magma body inside Tyrrhena Patera could conduct heat through the upper layers of the volcano that would melt any ice accumulation on the flanks, potentially triggering cata-

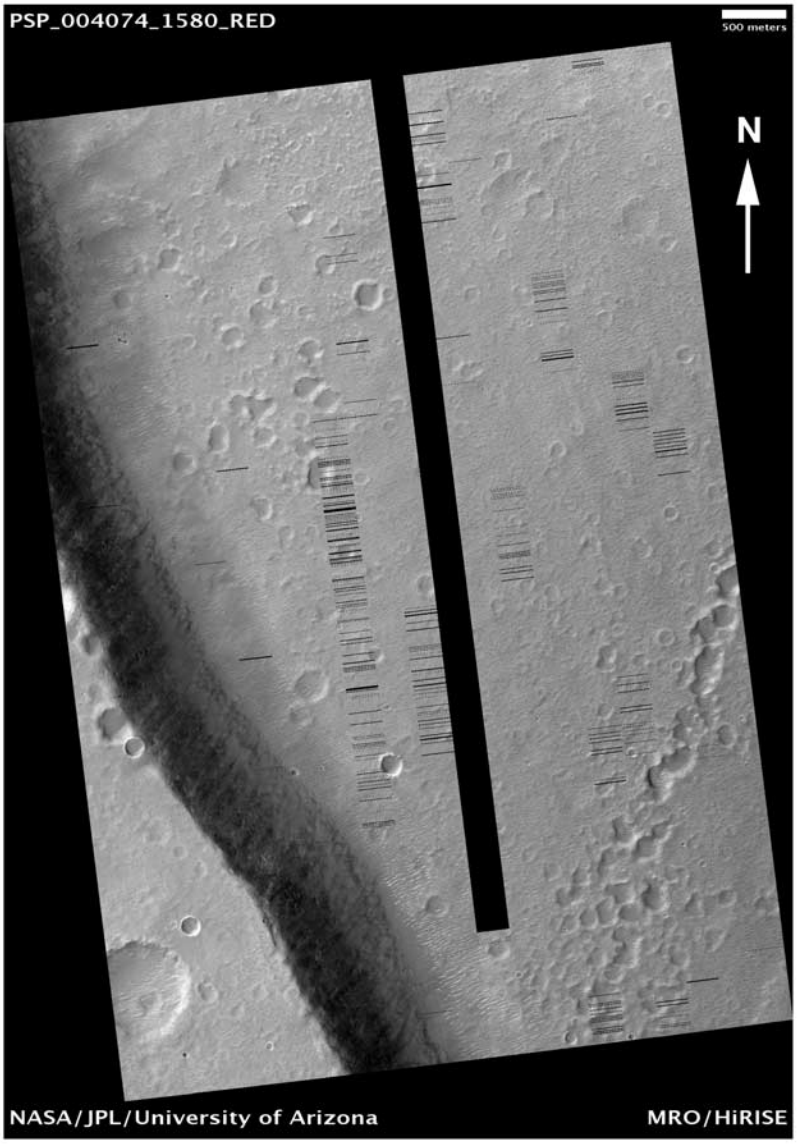

Figure 9. HiRISE image PSP_004074_1580 of the caldera rille floor material (unit AHrf) of *Gregg et al.* [1998]. This region is located along the western wall of the NW-trending elliptical depression that is a wide spot in the rille, downstream from the summit caldera. At full HiRISE resolution (30 cm/pixel), the surface of the rille floor is covered by linear duneforms, trending ENE, as found on the summit. However, approaching the rille's western wall, the surface become increasingly rocky, containing meter-scale boulders that have eroded out of the rille wall. We observed no unequivocal layering in this part of the rille wall. Although this unit was mapped by *Gregg et al.* [1998] as late-stage lava flows from the summit of the Tyrrhena Patera volcano, we observe no evidence of lava flow margins on the rille floor. If they exist, they have been buried by material deposited by subsequent aeolian activity. The chain of filled pits at lower right of the image is, however, reminiscent of crater chains marking the location of a lava tube [e.g., *Greeley*, 1971] or alternatively a chain of secondary impact craters. Scale bars is 500 m. Image courtesy of HiRISE Team.

strophic flooding and channel formation [cf., *Fassett and Head*, 2006].

[25] Second, it is important (and perhaps key) to remember that the Tyrrhena Patera edifice is thought to be composed of multi-layered, differentially welded and compacted ignimbrite deposits. Welded ignimbrites could exhibit zones with a wide range in physical properties and resistance to erosion [*Schmincke*, 2004], some behaving like solid igneous rocks and others like unconsolidated airfall deposits. Variation in the degrees of induration and welding of different pyroclastic layers composing the Tyrrhena Patera edifice would enable differential erosion of these layers by most types of processes. We suggest that the 1.2 Ga resurfacing event on unit Ns could be a result of differential erosion of pyroclastic layers with different degrees of induration and welding, which could explain

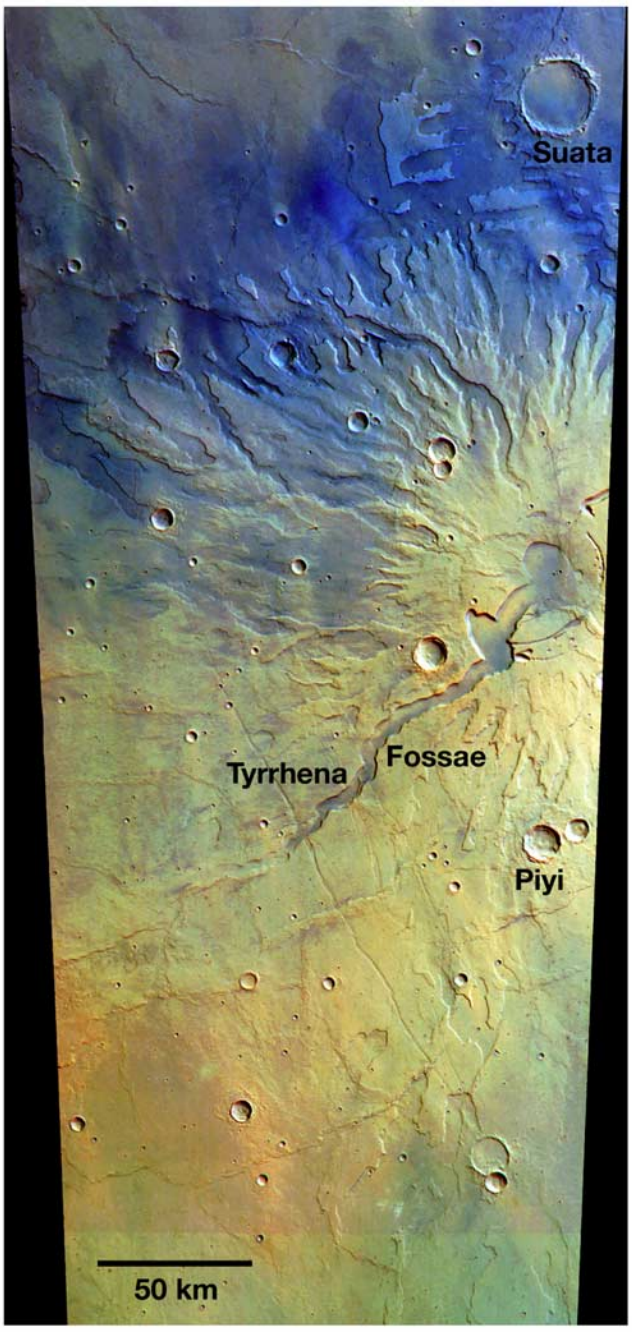

Figure 10. HRSC R-G-B color imaged (stretched) of Tyrrhena Patera volcano, produced using the red, green, and blue channels of orbit 440 data at 144 m/pixel. Note the channel floors contain a lower albedo material, which we suggest is basaltic volcanic fragments, perhaps with coarser particle sizes exposed by fluvial erosion or concentrated by aeolian removal of fines. This interpretation is consistent with studies of similar exposures of dark material observed in HRSC color data [*McCord et al.*, 2007].

why unit Ns was affected but not any of the other edifice-building units. As to the erosion mechanism, the northern part of unit Ns has a channeled topography in the THEMIS mosaic (Figure 1) and the HRSC image (Figure 2) consistent with fluvial erosion, which suggests that fluvial erosion is a likely but not a definitive candidate. The greater local slopes associated with areas of concentrated channeling might extend erosion of the flank materials from the Hesperian to the Amazonian in select localities. The HRSC color image (Figure 10) also shows a dark material in topographic lows, such as channel floors and outwash plains. This dark material, wherever it has been studied with the HRSC color data, has a spectral signature consistent with basaltic material [*McCord et al.*, 2007]. We suggest that this material is basaltic sand and dust deposited in topographic lows by aeolian or fluvial processes, perhaps eroded out of the Tyrrhena Patera edifice. The Hesperian to Early Amazonian formation age for unit AHrf is consistent with the Late Hesperian to Early Amazonian ages derived for the lava flow field extending to the SW from Tyrrhena Patera's flank [*Crown et al.*, 1992; *Mest and Crown*, 2001], indicative of long-lived volcanic activity at Tyrrhena Patera and for a transition from dominantly explosive to dominantly effusive eruptions.

[26] 3. *Nature of the 0.8 Ga Resurfacing Event:* The youngest measurable cratering model age on the Tyrrhena Patera volcano is a resurfacing age that occurs on three units: the upper shield Nsu (Figure 8), the caldera rille AHrf (Figure 9), and the channel floor AHcf. What kind of geologic event(s) could affect these three units but not others? The event would have to resurface the upper shield in all directions, as well as the caldera rille, but also cause resurfacing in the channels that then feed the channel floors north of unit Ns. For all three units with the 0.8 Ga age, the craters that were removed (and reaccumulated after the event) are in the 200–500 m diameter range. Using the following equations from *Garvin et al.* [1999]:

$$d = 0.12D^{0.96} \quad (1)$$

$$h = 0.03D^{0.96} \quad (2)$$

in which d is crater depth (m), D is crater diameter (m), and h is crater rim height (m), we find that the resurfacing event needed to obliterate craters with these diameters had to fill the craters to depths of ~20–50 meters, or erode craters with rim heights of 5–12 meters. We note that the surface of these units look extensively modified by aeolian activity (i.e., containing extensive dune fields, subdued topography, etc.); thus, some combination of infilling and erosion of crater rims could explain this cratering model age.

[27] Available HiRISE images of Tyrrhena Patera (Figures 5–9) show scattered dune fields and dust over cratered and pitted terrain, and individual layers in the walls of scarps have not yet been clearly resolved. We suggest that the simplest explanation is that an erosional event occurred at 0.8 Ga. As discussed above, units Nsu, AHrf, and AHcf are relatively flatter surfaces compared to the other Tyrrhena Patera units, such that preferential (aeolian?) erosion could have removed or obscured craters in the 200–500 m diameter range. Alternatively, an explosive volcanic eruption, centered on the caldera, could have occurred at Tyrrhena Patera ~0.8 Ga, in which column collapse triggered pyroclastic flows that spread relatively evenly across the shield. Simultaneously or shortly thereafter, the eruption

could have enabled melting of any ice on the flanks, or triggered the release of groundwater in the volcano, that would have flowed down the existing caldera rille and channels, perhaps eroding underlying material or depositing lahars (mud flows). Nevertheless, whether aeolian, volcanic, and/or fluvial activity caused the 0.8 Ga resurfacing event, high-resolution images show that the present surface of Tyrrhena Patera (Figures 5–9) has been modified by late-stage, differential aeolian erosion and deposition that has clearly been operating over the last billion years of Martian history [see also *Williams et al.*, 2007], and masked any evidence of lava flow margins in the caldera rille and fine-scale layering in scarp walls.

[28] If the 800 Ma age of the caldera rille floor and upper shield units marks the final stage of volcanism at Tyrrhena Patera, then this result has implications for the longevity of the magma sources in the Hellas region. None of the other highland paterae in the Circum-Hellas Volcanic Province [*Greeley et al.*, 2007; *Williams et al.*, 2008] has evidence of volcanic activity this late in Martian history (e.g., there is no evidence for major geologic activity at Hadriaca Patera later than ~1.5 Ga [*Williams et al.*, 2007].) Regardless, volcanic activity at the highland paterae ended long before volcanism in the Tharsis region, in which the Tharsis volcanoes experienced effusive volcanic activity as recently as ~100–300 Ma [*Neukum et al.*, 2004b].

[29] There are still unanswered questions regarding the geologic activity at Tyrrhena Patera. Future studies should utilize new data sets such as the MEX OMEGA and MRO CRISM spectrometers to investigate the compositions of materials on and around Tyrrhena Patera, MEX MARSIS and MRO SHARAD to image subsurface layers, and more extensive targeting of the MRO HiRISE camera should attempt high-resolution imaging of scarps on the shield flanks to assess the presence of, morphology, and thickness of potential layers. These observations could provide insight into the nature of individual eruption events and the role of hypothesized pyroclastic flows. However, it may require in situ measurements by robotic rovers to detect lava flows or individual pyroclastic layers to understand better the volcanic activity at Tyrrhena Patera.

7. Conclusions

[30] We assessed the geologic history of the Tyrrhena Patera volcano using crater counts on *Mars Express* HRSC images to determine cratering model ages for the material units defined in the *Viking Orbiter*-based geologic mapping of *Gregg et al.* [1998]. Our cratering model ages are generally consistent with their stratigraphy. Three intervals of major activity at Tyrrhena Patera have been identified: (1) formation of the volcanic edifice in the Noachian Period, ~3.7–4.0 Ga, after the Hellas impact (~4 Ga) and coincident with the formation of Hadriaca Patera (~3.9 Ga); (2) modification of the edifice and formation of the caldera rille and channels in the Hesperian Period; and (3) a final stage of modification in the Late Amazonian Epoch, ~0.8–1.4 Ga. The early- to mid-Hesperian activity on Tyrrhena Patera is coincident with similar activity on Hadriaca Patera at ~3.3–3.7 Ga. The youngest event on Tyrrhena Patera is modification on the upper shield, caldera rille, and channel floors at ~800 Ma. We speculate that a widespread process(es) is responsible for the coincidence of resurfacing in the three units. The most reasonable explanation is preferential (aeolian?) erosion of small craters on these flatter surfaces relative to the other units, or alternatively, some combination of pyroclastic flow emplacement on the upper shield and fluvial activity in the caldera rille and channels, followed by differential aeolian erosion and deposition, resulted the present surface. Unlike the Tharsis shields, major geologic resurfacing ended at Tyrrhena Patera nearly a billion years ago.

[31] **Acknowledgments.** The authors thank Tracy Gregg and Scott Mest for their very helpful reviews that improved the quality of the manuscript. We thank the HRSC Experiment Teams at DLR Berlin and the Freie Universität Berlin as well as the *Mars Express* Project Teams at ESTEC and ESOC for their successful planning and acquisition of data, as well as for making the processed data available to the HRSC Team. We acknowledge the effort of the HRSC co-investigator team members and their associates who have contributed to this investigation in the preparatory phase and in scientific discussions within the Team. Stephanie Werner and Gerhard Neukum were supported by DFG, the German Science Foundation. David Williams and Ron Greeley were supported by NASA through the Jet Propulsion Laboratory for US participation in the ESA *Mars Express* mission and through the NASA Planetary Geology and Geophysics Program.

References

Christensen, P. R., et al. (2004), The Thermal Emission Imaging System (THEMIS) for the Mars 2001 Odyssey mission, *Space Sci. Rev.*, *110*, 85–130.

Crater Analysis Techniques Working Group (1979), Standard techniques for presentation and analysis of crater size-frequency data, *Icarus*, *37*, 467–474.

Crown, D. A., and R. Greeley (1993), Volcanic geology of Hadriaca Patera and the eastern Hellas region of Mars, *J. Geophys. Res.*, *98*, 3431–3451.

Crown, D. A., and R. Greeley (2007), Geologic map of MTM-30262 and -30267 quadrangles, Hadriaca Patera region of Mars, *U.S. Geol. Surv. Sci. Inves. Ser. Map 2936*, 1:1,004,000.

Crown, D. A., T. K. Porter, and R. Greeley (1991), Physical properties of lava flows on the southwest flank of Tyrrhena Patera, Mars, in Abstracts of papers submitted to the 22nd Lunar and Planetary Science Conf., LPI, Houston, pp. 261–262.

Crown, D. A., K. H. Price, and R. Greeley (1992), Geologic evolution of the east rim of the Hellas basin, Mars, *Icarus*, *100*, 1–25.

Crown, D. A., D. C. Berman, L. F. Bleamaster, F. C. Chuang, and W. K. Hartmann (2005), Martian highland paterae: Studies of volcanic and degradation histories from high-resolution images and impact crater populations [CD-ROM], in *Lunar and Planetary Science Conference XXXVI*, Abstract 1476, Lunar and Planetary Institute, Houston.

Fassett, C. I., and J. W. Head (2006), Valleys on Hecates Tholus, Mars: Origin by basal melting of summit snowpack, *Planet. Space Sci.*, *54*, 370–378.

Garvin, J. B., S. E. H. Sakimoto, C. Schnetzler, and J. J. Frawley (1999), Global geometric properties of Martian impact craters: A preliminary assessment using Mars Orbiter Laser Altimeter (MOLA) [CD-ROM], in *Fifth Mars Conference*, Abstract 6163, Lunar and Planetary Institute, Houston.

Greeley, R. (1971), Lava tubes and channels in the lunar Marius Hills, *The Moon*, *3*, 289–314.

Greeley, R., and D. A. Crown (1990), Volcanic geology of Tyrrhena Patera, Mars, *J. Geophys. Res.*, *95*, 7133–7149.

Greeley, R., and P. D. Spudis (1981), Volcanism on Mars, *Rev. Geophys. Space Phys.*, *19*, 13–41.

Greeley, R., D. A. Williams, R. L. Fergason, R. O. Kuzmin, J. Raitala, G. Neukum, D. Baratoux, P. Pinet, L. Xiao, and the HRSC Team (2007), The Tyrrhena-Malea Volcanic Province, Mars, abstract presented at European Mars Science and Exploration Conference, p. 244, Noordwijk, Netherlands, 12–16 November, Abstract #1118874.

Gregg, T. K. P., and D. A. Crown (2004), Basaltic pyroclastic flows at Tyrrhena Patera and Hesperia Planum, Mars, abstract presented at IAVCEI Geneneral Assembly, Int. Assoc. of Volcanol. and Chem. of the Earth's Inter., Pucon, Chile.

Gregg, T. K. P., and M. A. Farley (2006), Mafic pyroclastic flows at Tyrrhena Patera, Mars: Constraints from observations and models, *J. Volcanol. Geotherm. Res.*, *155*, 81–89.

Gregg, T. K. P.,D. A. Crown, and R. Greeley (1998), Geologic map of part of the Tyrrhena Patera region of Mars (MTM-20252), *U.S. Geol. Surv. Misc. Inv. Ser. Map I-2556*, 1:500,000.

Hartmann, W. K. (1966), Martian cratering, *Icarus*, *5*, 565–576.

Hartmann, W. K. (2005), Martian cratering 8: Isochron refinement and the chronology of Mars, *Icarus*, *174*, 294–320.

Hartmann, W. K. (2007), Mars: Toward resolution of the controversy about small craters [CD-ROM], in *Lunar and Planetary Science XXXVIII*, Abstract #1060, Lunar and Planetary Institute, Houston.

Hartmann, W. K., and G. Neukum (2001), Cratering chronology and the evolution of Mars, *Space Sci. Rev.*, *96*, 165–194.

Hartmann, W. K., G. Neukum, and S. Werner (2008), Confirmation and utilization of the "production function" size-frequency distributions of Martian impact craters, *Geophys. Res. Lett.*, *35*, L02205, doi:10.1029/2007GL031557.

Ivanov, B. A. (2001), Mars/Moon cratering rate ratio estimates, *Space Sci. Rev.*, *96*, 87–104.

Jaumann, R., et al. (2007), The high-resolution stereo camera (HRSC) experiment on *Mars Express*: Instrument aspects and experiment conduct from interplanetary cruise through the nominal mission, *Planet. Space Sci.*, *55*, 928–952.

Levenberg, K. (1944), A method for the solution of certain problems in least squares, *Q. Appl. Math.*, *2*, 164–168.

Malin, M. C., K. S. Edgett, L. V. Posiolova, S. M. McColley, and E. Z. Noe Dobrea (2006), Present-day impact cratering rate and contemporary gully activity on Mars, *Science*, *314*, 1573–1577.

Marquardt, D. (1963), An algorithm for least-squares estimation of nonlinear parameters, *SIAM J. Appl. Math.*, *11*, 431–441.

McCord, T. B., et al. (2007), *Mars Express* High Resolution Stereo Camera spectrophotometric data: Characteristics and science analysis, *J. Geophys. Res.*, *112*, E06004, doi:10.1029/2006JE002769.

McEwen, A. S., B. S. Preblich, E. P. Turtle, N. A. Artemieva, M. P. Golombek, M. Hurst, R. L. Kirk, D. M. Burr, and P. R. Christensen (2005), The rayed crater Zunil and interpretations of small impact craters on Mars, *Icarus*, *176*, 351–381.

Mest, S. C., and D. A. Crown (2001), Geology of the Reull Vallis region, Mars, *Icarus*, *153*, 89–110.

Michael, G., and G. Neukum (2007), Refinement of cratering model age for the case of partial resurfacing [CD-ROM], in *Lunar and Planetary Science XXXVIII*, Abstract #1825, Lunar and Planetary Institute, Houston.

Neukum, G. (1983), Meteoritenbombardement und Datierung planetarer Oberflächen, Habilitation dissertation for faculty membership, 186 pp., Ludwig-Maximilians Univ., München, Munich, Germany.

Neukum, G., and K. Hiller (1981), Martian ages, *J. Geophys. Res.*, *86*, 3097–3121.

Neukum, G., and D. U. Wise (1976), Mars—A standard crater curve and possible new time scale, *Science*, *194*, 1381–1387.

Neukum, G., R. Jaumann, and the HRSC Co-Investigator and Experiment Team (2004a), HRSC: The High Resolution Stereo Camera of *Mars Express*, in *Mars Express: The Scientific Payload*, edited by A. Wilson, *Eur. Space Agency Spec. Publ.*, ESA SP-1240, 17–36, ESA Pub. Div., Noordwijk, Netherlands.

Neukum, G., et al. (2004b), Recent and episodic volcanic and glacial activity on Mars revealed by the High Resolution Stereo Camera, *Nature*, *432*, 971–979.

Neukum, G., et al. (2007), The geologic evolution of Mars: Episodicity of resurfacing events and ages from cratering analysis of image data and correlation with radiometric ages of Martian meteorites [CD-ROM], in *Lunar and Planetary Science XXXVIII*, Abstract #2271, Lunar and Planetary Institute, Houston.

Oberst, J., et al. (2008), The imaging performance of the SRC on Mars Express, *Planet. Space Sci.*, *56*, 473–491.

Peterson, J. E. (1978), Volcanism in the Noachis-Hellas region of Mars, 2, *Proc. 9th LPSC*, 3411–3432.

Plescia, J. B., and R. S. Saunders (1979), The chronology of the Martian volcanoes, *Proc. 10th LPSC*, 2841–2859.

Schmincke, H.-U. (2004), *Volcanism*, 324 pp., Springer-Verlag, Berlin.

Schultz, P. H. (1984), Impact basin control of volcanic and tectonic provinces on Mars, LPSC XV, 728–9.

Scott, D. H., and M. H. Carr (1978), Geologic map of Mars, *USGS Misc. Inv. Ser. Map I-1083*, 1:25M.

Werner, S. C. (2005), The Martian crater size-frequency distribution and aspects of the evolutionary history of Mars, Ph.D. dissertation, Free University, Berlin, Germany. (Available at http://www.diss.fu-berlin.de/2006/33/indexe.html)

Werner, S. C., and G. Neukum (2003), The end of the heavy bombardment as reflected in the ages of Martian impact basins [CD-ROM], in *Lunar and Planetary Science XXXIV*, Abstract #1986, Lunar and Planetary Institute, Houston.

Williams, D. A., R. Greeley, W. Zuschneid, S. C. Werner, G. Neukum, D. A. Crown, T. K. P. Gregg, K. Gwinner, and J. Raitala (2007), Hadriaca Patera: Insights into its volcanic history from *Mars Express* High Resolution Stereo Camera, *J. Geophys. Res.*, *112*, E10004, doi:10.1029/2007JE002924.

Williams, D. A., et al. (2008), The Circum-Hellas volcanic province, Mars: Overview, *Planet. Space Sci.*, doi:10.1016/j.pss.2008.08.010.

D. A. Crown, Planetary Science Institute, 1700 East Ft. Lowell Road, Suite 106, Tucson, AZ 85710, USA.

R. Greeley and D. A. Williams, School of Earth and Space Exploration, Arizona State University, Box 871404, Tempe, AZ 85287-1404, USA. (david.williams@asu.edu)

G. Michael and G. Neukum, Department of Earth Sciences, Institute of Geological Sciences, Planetary Sciences and Remote Sensing, Freie Universität Berlin, Malteserstr. 74-100, Building D, D-12249 Berlin, Germany.

J. Raitala, Astronomy Division, Department of Physical Sciences, University of Oulu, P.O. Box 3000, FIN-90401 Oulu, Finland.

S. C. Werner, Geological Survey of Norway (NGU), Leiv Eirikssons vei 39, N-7491 Trondheim, Norway.